Progress in Organic Coatings 183 (2023) 107760

Contents lists available at ScienceDirect

Progress in Organic Coatings

journal homepage: www.elsevier.com/locate/porgcoat

Ultrasonic spray deposition of PEGDE-crosslinked chitosan/graphene oxide coatings for enhancing gas barrier properties of polybutylene succinate films

Alessia Cabrini [a,b], Arash Ghalayani Esfahani [a], André Petraconi [f], Marino Lavorgna [a,c,*], Luigi De Nardo [b], Giovanna Giuliana Buonocore [c], Ricardo Jorge Espanhol Andrade [e,f], Pierfrancesco Cerruti [a,d]

[a] Institute of Polymers, Composites and Biomaterials UOS Lecco, National Research Council, Via Previati 1/C, 23900, Lecco, Italy
[b] Department of Chemistry, Materials and Chemical Engineering "G. Natta", Politecnico di Milano, Milano, Italy
[c] Institute for Polymers, Composites and Biomaterials, National Research Council of Italy, P. le Fermi, 1-80055, Portici, Naples, Italy
[d] Institute for Polymers, Composites and Biomaterials, National Research Council of Italy, via Campi Flegrei, 34, 80078 Pozzuoli, Naples, Italy
[e] MackGraphe - Mackenzie Institute for Research in Graphene and Nanotechnologies, Rua da Consolação, 896, SP, 01302-907 São Paulo, Brazil
[f] Engineering School, Mackenzie Presbyterian University, Rua da Consolação 896, São Paulo 01302-907, Brazil

ARTICLE INFO

Keywords:
Nanocomposite coatings
Ultrasonic spray coating
Chitosan
Graphene oxide
Gas barrier properties

ABSTRACT

Biobased and biodegradable polymers represent a valid and sustainable alternative to oil-based plastics, as they are renewable and address the issue related to the end-of-life of non-compostable materials. However, the poor gas barrier of biopolymers limits their use in several applications, including food packaging.

In this work, chitosan/graphene oxide (CS/GO) nanocomposite coatings were successfully deposited by ultrasonic spray on a compostable polybutylene succinate (PBS) film. The moisture resistance of the chitosan coatings was improved by crosslinking with polyethyleneglycol diglycidyl ether (PEGDE). The resulting coatings were transparent, with thickness in the 1–2.5 μm range, and exhibited good adhesion to the PBS film and mechanical and scratch resistance due to the presence of GO nanofiller. In detail, the PEGDE-crosslinked CS/GO (CS/PEGDE/GO) nanocomposite coating containing 1 wt% GO allowed to reduce O_2 and CO_2 transmission rates by 85 % and 93 %, respectively, compared to uncoated PBS film. The permeability reduction is ascribed to the formation of compact coatings with GO nanoplates oriented parallel to the PBS substrate. Furthermore, the improvement in CO_2 barrier properties was up two-time more than that related to oxygen, suggesting the use of CS/PEGDE/GO coatings in applications where gas permselectivity is required. This research demonstrates the potential of the ultrasonic spray technique for producing bionanocomposite barrier coatings with improved gas barrier performance.

1. Introduction

The food packaging industry is increasingly turning to biobased and biodegradable polymers as substitutes for conventional and fossil-based plastics. This interest arises from growing environmental concerns related to the end-of-life management of non-compostable materials and evidence that only low percentages of plastic waste are currently recycled [1,2]. In this scenario, polylactide (PLA), which is a biodegradable polymer, is widely used in the manufacture of rigid packaging due to its high thermal stability, good transparency and processability, while showing some limitations such as low mechanical properties and weldability when applied to flexible packaging [3]. An alternative and promising candidate for the production of biodegradable films for flexible packaging is poly (butylene succinate) (PBS) due to its excellent processability by conventional industrial techniques and its favorable mechanical and thermal properties. [4]. However, the use of PBS in packaging is limited because of its lower gas and moisture barrier properties than conventional plastics [5].

Coating technology has been proposed as a promising strategy to broaden the application range of mono-material films and, in turn,

* Corresponding author at: Institute of Polymers, Composites and Biomaterials UOS Lecco, National Research Council, Via Previati 1/C, 23900, Lecco, Italy.
E-mail address: marino.lavorgna@cnr.it (M. Lavorgna).

https://doi.org/10.1016/j.porgcoat.2023.107760
Received 28 February 2023; Received in revised form 15 May 2023; Accepted 14 June 2023
Available online 28 June 2023

reduce the need for multilayer packaging, which ensures high technological performance (i.e., weldability, low gases permeability, etc.) but exhibits poor sustainability [6,7]. The deposition of a functional thin layer based on a biodegradable and bio-based polymer matrix allows for maintaining the biodegradability characteristics of compostable packages, whereas the addition of two-dimensional (2D) nanofillers may significantly reduce the gas permeability thanks to the increment of diffusion paths [8,9]. Many works have proved that nanoplates appropriately dispersed in polymer matrices, such as graphene [10], graphene oxide (GO) [11], and nanoclays [12], force gas molecules to follow longer and tortuous paths to cross the material. Moreover, the gas barrier performance of nanocomposite depends on the optimization of several parameters, such as nanofiller characteristics (aspect-ratio, surface area, volume fraction) and filler-polymer interactions (such as filler dispersion, spatial distribution, and orientation) [13].

This study focuses on investigating bionanocomposite coatings made of chitosan (CS) and GO nanoplates that are dispersed in the CS matrix. Chitosan is a natural polymer obtained mainly by the deacetylation process from chitin, the second most abundant polysaccharide on earth [14]. In the last decades, CS has been widely employed to produce films and coatings for many applications, including food preservation, because of its intrinsic advantages, such as biodegradability, renewability, biocompatibility, and antimicrobial/antioxidant ability [15]. In addition, chitosan contains abundant reactive functional groups on its backbone, such as amine and hydroxyl groups, which can react via intermolecular hydrogen bonds and electrostatic interactions with anionic compounds and nanoparticles [16]. In several papers, chitosan has been coupled with clay nanoplatelets to improve the barrier properties of the substrate [17]. For instance, Laufer et al. [18] prepared thin films of chitosan and montmorillonite clay nanoplatelets via a layer-by-layer assembly by exploiting the opposite charge that characterizes the two materials and thus improving the oxygen permeability of a polylactic acid film by four orders of magnitude at 0 % RH. Nevertheless, the combination of GO, a high-aspect-ratio nanofiller characterized by various oxygen-containing groups, with chitosan has recently been reported in many papers as a viable approach to improve the chitosan's functional properties [19]. In this regard, Yan et al. [20] prepared chitosan-based films, containing 1.0 wt% boron as a crosslinker and 1.0 wt% GO as filler, via solvent casting and subsequent thermal treatment: the obtained composites showed enhanced tensile strength and oxygen permeability by ~160 and ~90 % compared to pristine chitosan, respectively. Ahmed et al. [21] incorporated GO into chitosan films through the solution casting method, and they observed a significant improvement in tensile strength, barrier properties, and glass transition temperature. Furthermore, Han Lyn et al. [22] prepared CS/GO nanocomposite films crosslinked using sodium tripolyphosphate with enhanced mechanical properties and water and oxygen barrier properties.

The low water resistance of natural biopolymers, such as chitosan, is a major obstacle to their industrial use due to their inherent hydrophilicity. However, research has shown that chemical crosslinking enhances the chemical stability of chitosan against water swelling effect. Among the possible crosslinking agent, poly(ethylene glycol) diglycidyl ether (PEGDE) has been largely proposed as a chitosan crosslinker for biomedical applications [23–25] and it is recognized as safe by the Food and Drug Administration [26]. As far as is currently evident from literature, there are currently no published articles on the use of PEGDE as a crosslinker for food packaging or CS/GO nanocomposite coatings.

Various techniques have been employed to apply nanocomposite coatings, including bar coating [27], LbL assembly [28], and spray coating [29] deposition approaches. Currently, to the best of authors knowledge, there are no studies that have examined the use of ultrasonic spray technology to deposit polymer-based composite dispersions. However, ultrasonic spray (USS) coating is a promising automated technique that offers several advantages such as: rapid and precise deposition with low material consumption, good reproducibility, the possibility of covering large surfaces, and potential scalability from research to volume production [30–37]. This technique relies on the principle of ultrasonic atomization, whereby high-frequency sound vibrations are used to produce a fine mist of the sprayed mixture. The mist is composed of microdroplets with a very narrow size distribution [30]. In turn, the small dimensions and their uniform size distribution enable the manufacturing of homogenous and thin coating layers. Also, the ultrasound pulses break the agglomerates in the suspension, promoting a homogeneous dispersion of particles [31]. In recent years, this emerging technology has been exploited to deposit different nanoparticles or solutions for various purposes. Bose et al. [32] performed a systematic study to analyze the influence of several factors related to the spaying materials and process on the formation of homogeneous polymer films. Using a mathematical model, they define two regimes, "dry" and "wet," and a narrow intermediate region between these two where they obtained high-quality films (i.e., uniform thicknesses and low roughness). USS coating has been exploited to improve the surface quality of additive manufactured items [33], to produce graphene-coated smart textiles [34], fuel cell electrodes [35], and electrochromic windows [36]. Recently, Abbas et al. [37] have produced ZnO nanoparticle (NP) coatings to improve the oxygen and UV barrier properties of poly (ethylene terephthalate) (PET) and poly(3-hydroxybutyrate-*co*-3-hydroxy hexanoate) (PHBHHx) substrates. Although the coating was ineffective in improving the oxygen barrier performance, the ZnO NPs layer created a good blocking layer against light in the UVA region.

In this work, chitosan-based nanocomposite coatings containing GO and PEGDE as crosslinkers were successfully prepared by using the USS coating technique. The effect of GO volume fraction in chitosan matrix and coating thickness on gas barrier properties was investigated by depositing different CS/PEGDE/GO coatings on PBS films. Chemical, thermal, and physical characterizations were performed to optimize the crosslinking conditions and coating formulations. Gas barrier properties measurements highlighted a drastic reduction in oxygen and carbon dioxide transmission, which were significantly influenced by the thickness and GO content, and a possible tuning of the two gas permeability ratios. Morphological characterization of nanocomposite coatings showed an effective GO nanoplates orientation parallel to the substrates, which is ensured by the USS deposition technique. Moreover, the coating adhesion and mechanical and scratch resistance result to be improved by the presence of GO.

2. Materials and methods

2.1. Materials

Medium molecular weight chitosan (CS) in powder form (deacetylation degree >75 %), diepoxyPEG (diePEG, MW = 500, epoxy conversion ~95÷98 %), and acetic acid were all supplied by Sigma-Aldrich (Italy). To prepare the graphene oxide nanosheets, graphite flakes (Qingdao Dahe Graphite Co. Ltd., China) was used according to the Hummers method, which has been described in previous studies [20]. Flexible PBS film of 100 μm thickness was provided by Corapack (Como, Italy).

2.2. Preparation of coating dispersions

GO was dispersed in water (1 mg/ml) using ultrasound tip sonication for 2 h. Chitosan solution (1 % *w/v*) was prepared by dispersing CS powder in 0.4 % v/v acetic acid solution (pH = 4.2) under stirring for 24 h at room temperature. The resulting solution was then filtered to remove undissolved particles. The GO/CS dispersions were prepared by adding different amounts of GO dispersion to the CS solution under vigorous stirring (0.5, 1, and 2 % w/w). Then, PEGDE was added dropwise to the GO/CS mixture and stirred at 80 °C overnight. The crosslinker concentration and coating formulations were optimized by preparing and characterizing free-standing films. Three PEGDE

concentrations were compared by considering a -NH_2:epoxy group ratios equal to 5:1, 4:1, and 3:1 (23 wt%, 29 wt%, and 38 wt% based on chitosan weight, respectively), which were coded as CS/PEGDE 5:1, CS/PEGDE 4:1, and CS/PEGDE 3:1. Films thick around 40 μm were prepared by solvent casting at room temperature and kept in a desiccator until their characterization.

2.3. Coating realization by USS deposition

Prior to coating, the PBS film was rinsed with distilled water and ethanol, and then plasma-treated using plasma surface technology in air (Diener Pico), for 20 min, at 90 μA and 0.4 mbar. The coating dispersion was deposited using a SimCoat Ultrasonic Spray Coater (SONO-TEK) (Fig. S1a) equipped with an Impact nozzle. The latter is connected to a programmable syringe pump, which feeds the dispersion with a constant flow rate. The generator creates ultrasound vibrations inside the nozzle, forcing the suspension to move as capillary waves. Upon reaching the tip of the nozzle, the waves acquire a large enough amplitude to break into a fine mist of droplets, shaped and directed towards the substrate by the pressure-controllable jet air deflector (positioned above the nozzle). An x-y stage controls the nozzle movement (the nozzle path is shown in Fig. S1).

Different types of coatings have been deposited on the selected substrate to highlight the effect of both coating thickness and layered structure (i.e., 1-, 2-, and 3-layers were deposited to prepare a multi-layered coating) and GO content (i.e., 0, 0.5, 1, 2 wt% on chitosan weight). Drying of each deposited layer was carried out at room temperature under a hood for 20 min before depositing the successive layer. Table 1 summarizes the prepared samples and their multi-layer structure.

To compare USS coating technique with another deposition technique, the sample coded CS/PEGDE/1%GO_1L (Table 1) was also prepared by traditional air spray coating because of the similarity between the two processes. The same coating mixture amount, spraying path, and nozzle speed were used and the mixture was deposited in a single deposition cycle. Following some preliminary tests, the air pressure was set at an overpressure of 0.68 bar, thus much higher than that for ultrasonic spray coating, where the pressure was 0.03 bar.

2.4. Characterization of coatings and coated films

Fourier-transform infrared (FTIR) spectra of films were recorded by attenuated total reflection (ATR) mode with an FTIR spectrometer (Nicolet iS 10, Thermo Fisher Scientific, Waltham, MA) at room temperature. Infrared spectra were recorded from 500 to 4000 cm^{-1}, performing 32 scans at 1 cm^{-1} resolution.

Thermo gravimetric analysis (TGA) was carried out using a TG-SDTA 851 thermobalance (Mettler-Toledo, Milan, Italy). The measurements were performed on samples of approximately 3.5 mg, which were heated from 25 to 800 °C at a rate of 5 °C/min in nitrogen (30 ml/min).

The water stability of PEGDE/CS films was evaluated by water swelling tests. The specimens were weighed and placed in Petri dishes filled with Phosphate Buffer Saline (PBS, NaCl 120 mM, KCl 2.7 mM, Na_2HPO_4 10 mM, pH 7.4) solution. At selected time points (1, 2, 7, 14, 21, and 28 days), specimens were weighed after carefully removing the excess liquid. The percentage of water uptake (WU) was calculated using Eq. (1):

$$WU\ (\%) = \frac{w_t - w_0}{w_0}\ x\ 100 \quad (1)$$

where w_t and w_0 are the wet weight at time t and the dry weight at time 0, respectively.

The morphological analysis was conducted on an FEI Quanta 200 FEG Scanning Electron Microscope (SEM) (FEI, Eindhoven, Netherlands) at an acceleration voltage of 5–10 kV. Before the observation, the specimens were cryogenically fractured in liquid nitrogen, and their surface was sputter coated with Au—Pd alloy to make them conductive, using a BalTec MED020 unit. Surface and cross-sectional images were acquired: the latter were analyzed using ImageJ software to calculate the coating thickness. Transmission electron microscopy (TEM; Hillsboro, OH, USA) images were obtained on FEI TECNAI G12 Spirit-Twin operating at 120 kV and LaB6 source. The microscope was equipped with an FEI Eagle 4 K CCD camera and NanoImaging Services Software (v4, San Diego, CA, USA).

The surface morphology of the film and the distribution of GO were analyzed using atomic force microscopy (AFM, Dimension Icon® Bruker). Soft tapping mode stabilized by amplitude–modulation feedback was used to acquire topographies, and the Asyst-Air probe was employed. The obtained images were analyzed with Gwyddion software.

Oxygen and carbon dioxide transmission rates of coated PBS films were measured in accordance with ASTM-3985 by using $PermeO_2$ and Multiperm permeation devices, respectively (ExtraSolution, Lucca, Italy). The films, with an exposed surface area of 50 cm^3, were tested at atmospheric pressure. Duplicate measurements were performed at 25 °C at 0 % and 50 % relative humidity (RH).

Nanoindentation and nanoscratch tests were performed with a NanoTest Platform Two by Micro Materials Ltd., using a three-sided pyramidal (Berkovich) diamond indenter. For the nanoindentation test, the measurements were performed by setting the maximum load during the loading phase at 0.5 mN and holding it for 60 s before unloading. The load applied by the indenter was linearly increased with a rate of 0.5 $nNs^{-1,}$ recording the tip displacement in the normal direction to the coating surface. To evaluate the statistical distribution, 50 indentations were performed with a distance of 15 μm between adjacent indentations. Nanoscratch tests were performed to assess the abrasion and scratch resistance of the developed coatings. In this case, the indenter was driven to move tangentially over the surface with a scan rate of 0.0250 mN/s for 1 mm, while the tip normal load was linearly increased up to 25 nN.

The coating adhesion to the PBS substrate was evaluated through the cross-cut test described in ISO 2409. Using the Cross Hatch Cutter Model 295, a series of several cuts at right angles to form a square pattern were made, with sufficient pressure to reach the substrate. Then, an adhesive tape was applied to the square pattern and quickly removed by pulling it away with an angle of 60°. The coating-substrate adhesion was assessed by observing the coating appearance through optical microscopy. Tensile tests were performed on films conditioned for 48 h at 25 °C and 50 % RH, using an Instron model 5564 dynamometer equipped with a 1 kN load cell, at 23 ± 2 °C, 45 ± 5 % RH, with a 5 mm min^{-1} clamp separation rate. Four dog bone-shaped specimens (50 mm overall length, 28 mm distance between the wide parallel sections, 4 mm width) were tested for each formulation.

Table 1
Coatings formulations, structures, and measured thicknesses.

Sample code	GO content [wt %]	Number of layers	Coating thickness [μm]
CS/PEGDE_1L	0	1	0.88 ± 0.09
CS/PEGDE/1% GO_1L	1	1	0.91 ± 0.16
CS/PEGDE/1% GO_2L	1	2	1.46 ± 0.14
CS/PEGDE_3L	0	3	2.62 ± 0.07
CS/PEGDE/0.5% GO_3L	0.5	3	2.46 ± 0.11
CS/PEGDE/1% GO_3L	1	3	2.47 ± 0.31
CS/PEGDE/2% GO_3L	2	3	3.43 ± 0.20

3. Results and discussion

3.1. Physical and chemical characterization of free-standing films

PEGDE-crosslinked CS and CS/GO films were successfully prepared by solvent casting following a modified protocol reported by Kiuchi et al. [38]. The expected crosslinking mechanism involves the opening of the epoxy rings of PEGDE and their reaction with amino groups of CS, promoted by the reaction temperature at 80 °C (the reaction scheme is shown in Fig. S2). The selected reaction time was defined by FTIR analysis obtained by taking aliquots of the solution under stirring at progressive time intervals. ATR–FTIR spectra reported in Fig. S3 show a progressive reduction of the peak at 912 cm^{-1} corresponding to the bending vibration of the epoxy ring; the disappearance of the peak after 4 h of reaction indicates the complete conversion of the PEGDE epoxy group and consequently the completion of the crosslinking reaction.

ATR-FTIR spectra of CS and CS/PEGDE (Fig. 1a) show broadband in the 3600 to 3000 cm^{-1} range, corresponding to –OH and –NH stretching vibrations. In this region, two peaks with similar intensity appear at 3360 and 3266 cm^{-1} in CS film. The peak at 3266 cm^{-1}, attributed to the NH stretching vibration of primary amines, decreases in intensity compared to that at 3360 cm^{-1} in films containing PEGDE. This spectral feature confirms the occurrence of the reaction between chitosan amines and PEGDE epoxy groups. The main difference between the spectra of CS/PEGDE and pristine CS is observed in the spectral region between 1700 and 1500 cm^{-1}. The CS spectrum shows the characteristic bands at 1650 and 1565 cm^{-1}, which are associated with *N*-acetyl groups (C═O stretching of amide I) and -NH bending vibrations. However, the band at 1565 cm^{-1} can also be associated with amine groups as well as -NH3 + -OOCCH3 interactions [39], whereas the –NH deformation vibration in primary amine can be found at 1410 cm^{-1} [40]. Due to the cross-linking reaction with PEDGE, the intensity of the peak at 1565 cm^{-1} and 1410 cm^{-1} progressively decreases as the CS:PEGDE ratio decreases, while a new peak originates at 1587 cm^{-1}, attributed to the NH bending of secondary amines [41] or alternatively to the shift of primary amines peak by H-bonding interactions. These spectral evidences together with the disappearance of the bending vibration at 912 cm^{-1} of the epoxide ring (Fig. S4), confirms that the reaction between chitosan and PDGE is completed until the epoxide groups are depleted.

The ATR-FTIR spectra of the CS/PEGDE/GO coatings (Fig. 1b) are slightly different from those observed for the PEGDE-crosslinked CS films. In fact, only the peak at 1565 cm^{-1} appears in the spectral region of the amine groups, while the peak at 1590 cm^{-1} does not appear, confirming that a new network of interactions is created in the presence of GO, with additional interactions between chitosan and GO. Therefore, spectroscopic analysis shows no evidence of specific covalent interactions between PEGDE and GO, although this cannot be ruled out and this can be attributed to the greater reactivity of the epoxide ring with amines rather than hydroxyl groups [38,41].

Since the water uptake is strictly related to the physical structure of hydrophilic polymers, the swelling dynamic at neutral pH and room temperature was studied over two days for all prepared films (Fig. 2). A weight gains of about 6000 % is noted for CS after 1 h/soaking. After the second weight measurement, the CS specimens lost their structural integrity to prevent further weight measurements. Chitosan crosslinked with 23 % PEGDE showed a weight increase over 96 % lower than pristine chitosan (Fig. 2a), demonstrating improved resistance to water swelling. The observed water uptake reduction is in line with the literature concerning CS/PEGDE system [24,25], and it is attributed to the presence of crosslinks between epoxy and amino groups. This results in both a reduction of reactive hydrophilic groups and the formation of a more rigid structure, preventing network expansion. However, the increase of the PEGDE concentration from 23 wt% up to 38 wt% reduced the swelling rate to a low extent (15 % reduction observed for CS/PEGDE 3:1 compared to CS/PEGDE 5:1, Fig. 2b). This evidence can be justified considering that even for the higher concentration of PEGDE (38 wt%, -NH_2:epoxy group ratio equal to 3:1), two-thirds of the amines are not involved in crosslinking and can still interact with water molecules. Therefore, considering the relatively low stability increase towards water swelling and the higher cost, a PEGDE concentration of 23 wt% was selected for preparing crosslinked CS/GO nanocomposite coatings. It is worth noting that the films containing 0.5 and 1 wt% GO show a similar swelling rate of 23 wt% PEGDE, whereas samples containing 2 wt% GO show a slight increase in water uptake.

In order to further understand the role of crosslinking with different PEGDE concentrations on the water sensibility of CS and CS/GO systems, TGA was performed on CS, CS/PEGDE, and CS/PEGDE/GO films. The results of the analysis, discussed in detail in Section S1, pointed out a reduction in moisture content (corresponding to the weight loss in the first degradation stage) and an increase in the water evaporation temperature for all the PEGDE-crosslinked samples (Table S1 and Fig. S5). However, as observed for water uptake tests, the increase of PEGDE concentrations brings about only a slight reduction of chitosan's capability to absorb water molecules. Consequently, the choice to use the lowest concentration of PEGDE studied is further supported by the findings obtained from the TGA curves.

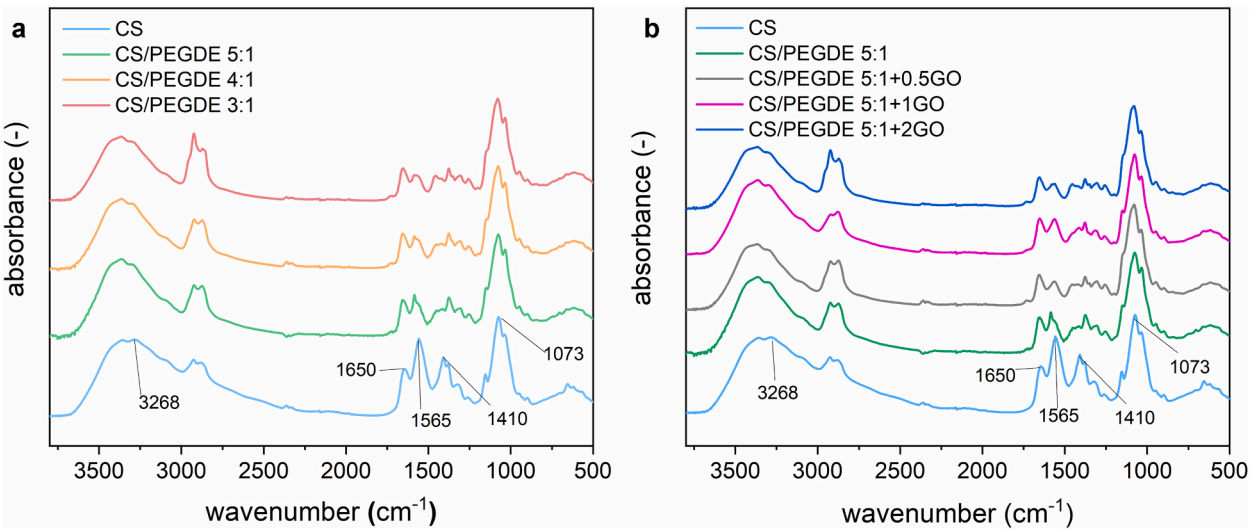

Fig. 1. FTIR spectra of (a) CS, CS/PEGDE films, and (b) CS/PEGDE/GO films.

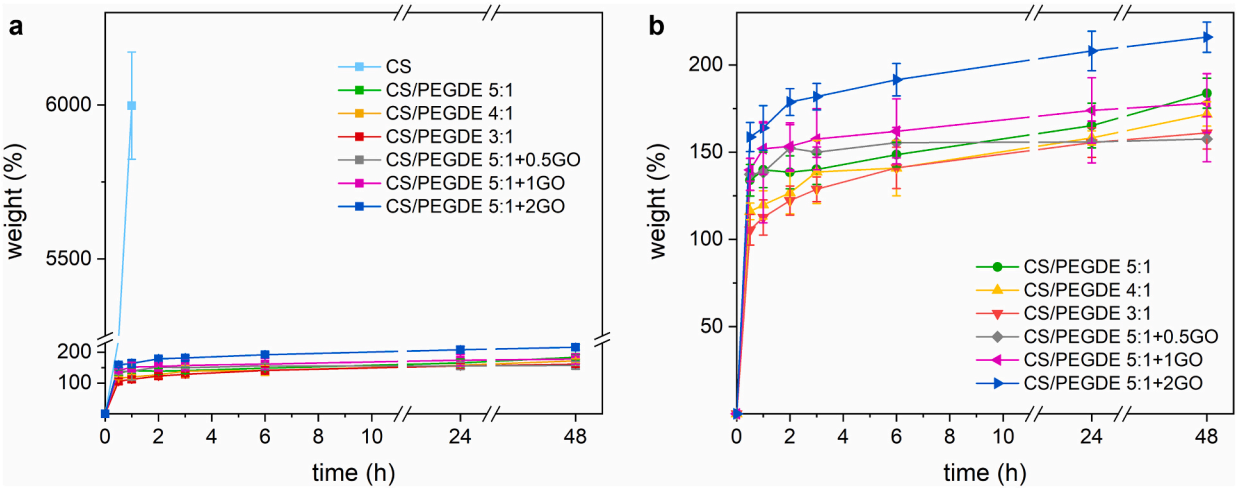

Fig. 2. Swelling profiles of CS, CS/PEGDE films (a), and of CS/PEGDE/GO films containing the selected PEGDE content (b) in PBS.

3.2. Wettability of the PBS substrate

To enhance the wetting properties and promote water-based coating adhesion, a low-pressure air plasma treatment was employed on the PBS films before the coating deposition. The wettability of plasma-treated PBS films was assessed through water contact angle (WCA) measurements performed immediately after the plasma (Fig. S6a). PBS films show a slight hydrophobic behavior with a WCA of 68.4°. Instead, plasma-activated films become hydrophilic, showing a WCA value of 22.3°. The FTIR spectra of PBS films were acquired to determine any modifications of the surface chemical structure (ATR-FTIR spectra of PBS before and immediately after plasma treatment are reported in Fig. S6b). Concerning pristine PBS, the following characteristic peaks can be highlighted [3]: the band at 2945 and 1330 cm^{-1} are assigned to –CH– asymmetric and symmetric stretching vibrations, respectively, while the sharp band at about 1709 cm^{-1} is attributed to the C═O stretching vibrations of the ester linkage. The peaks at about 1210 and 1150 cm^{-1} correspond to the –C–O–C– stretching in the ester bonds, while the band at 1044 cm^{-1} is related to the –O–C–C– stretching. Finally, the peak at 955 corresponds to the –C–OH bending in the carboxylic acid groups. It should be noted that the same characteristic peaks are also present in the activated films' spectra. However, a slight increase in 1710 cm^{-1} intensity is observed by increasing plasma treatment times due to the formation of oxidized species [42].

3.3. Morphological characterization of coatings

Ultrasonic spray coating was used to coat PBS films that had been activated by plasma. The efficacy of deposition depends on several material and process parameters that strongly influence the homogeneity of the developed coatings. Thus, they were suitably studied (Section S2) to identify the optimal parameters combination (Table S2) to achieve uniform material distribution. Using the optimized deposition conditions, homogenous coatings with varying thicknesses were prepared by building up a multi-layered structure (mono-, bi-, tri-layer). Each layer was prepared by selecting the minimum number of spraying cycles (defined as 4, Table S2) to achieve complete coalescence of the micro-droplets and formation of a continuous liquid layer. The choice was made to create thinner individual liquid layers and, thus, avoid the "ring-coffee" effect, which is common in the "wet" regime and that leads to the accumulation of nanocomposite in specific film areas upon solvent evaporation [32]. Macroscopic images reported in Fig. S8a–b show the deposition of a multilayer coating allows for a more homogeneous distribution of polymer and filler as compared to the monolayer coating with the same thickness. Furthermore, it is worth noticing that the coating layers affected the optical transmittance of PBS films to a low extent since a maximum transparency reduction of 5 % was noted for the tri-layer coatings in the entire visible range (Fig. 3).

Representative cross-sectional SEM images of CS/PEGDE/GO coatings and measured thicknesses of developed samples are reported in Fig. 4a–c and Table 1. The thickness of the CS/GO/PEGDE coatings increases almost linearly with the number of deposited layers. In addition, the cross-section images demonstrate the formation of a dense and compact layer without any visible pores or cracks. This indicates a high level of compatibility and interaction between the various layers that were deposited [43]. It is worth noting that the thickness further increases for the CS/PEGDE/GO coatings with the highest GO concentration. In fact, 3-layer coatings containing 2 wt% GO display an average thickness of 3.34 μm, compared to about 2.5 μm for the other 3-layer systems. As observed in other studies, this significant increment of coating thickness with the GO content is ascribed to the GO nanoplates stacking and agglomeration [23,44]. SEM surface micrographs of CS/PEGDE and CS/PEGDE/GO composites are illustrated in Fig. 4d–g. CS/PEGDE coatings have the most uniform and homogeneous surface. On the other hand, the surface of the CS/PEGDE/GO composite coatings is rough and exhibits circular features, more evident with increasing GO loadings, attributed to GO sheets agglomerates entrapped in the CS

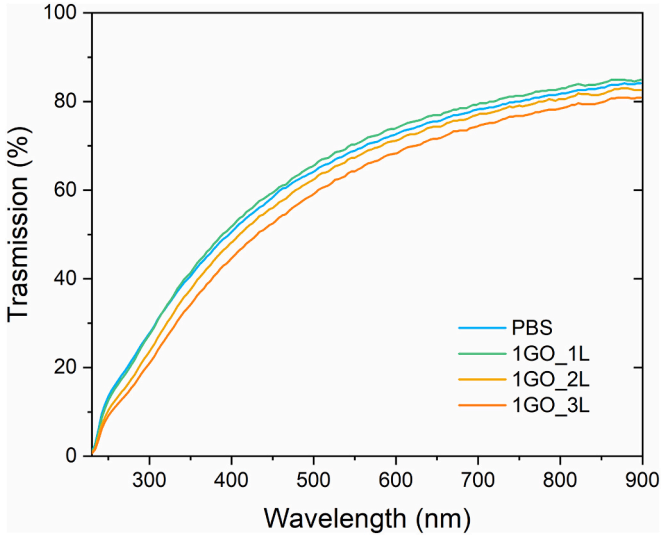

Fig. 3. UV–vis Spectrum of PBS pristine and coated with mono-, bi-, and tri-layer coatings, continuing 1 wt% of GO.

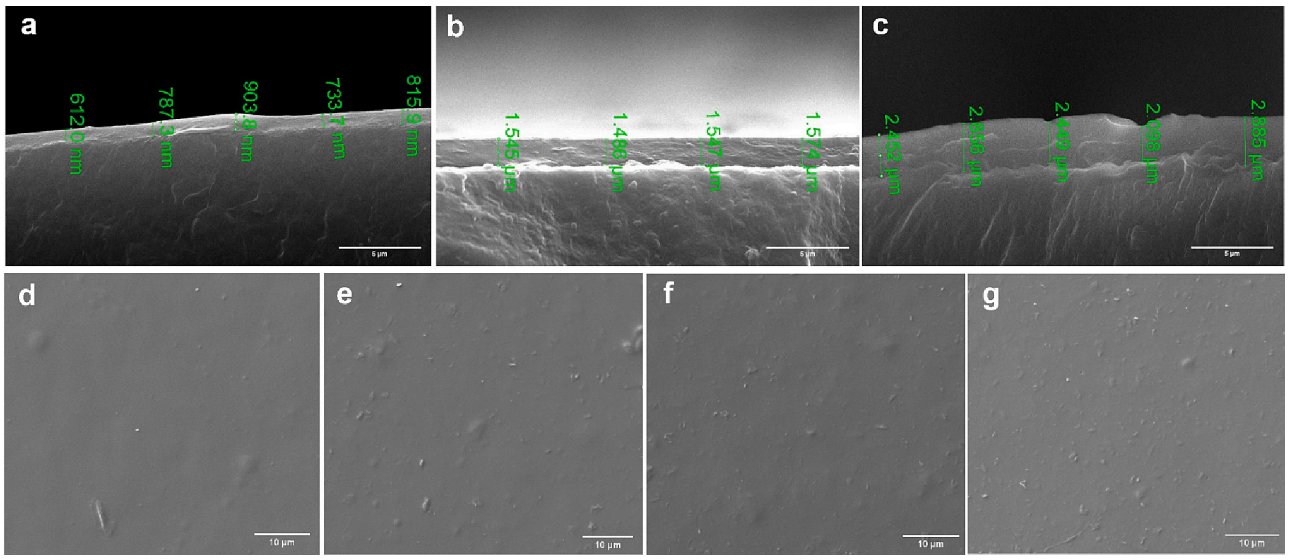

Fig. 4. SEM images of the cross-sections of 1-layer (a), 2-layer (b), and 3-layer (c) of CS/PEGDE/GO coatings (1 wt% GO). SEM images of the surface of 3-layer CS/PEGDE (d), and CS/PEGDE/GO coatings prepared with varying GO concentrations: 0.5 wt% (e), 1 wt% (f), 2 wt% (g).

matrix.

A similar change in the surface morphology of CS/GO nanocomposites with the increase of GO content was observed by Pan et al. [45] and Ahmed et al. [21]. This phenomenon is more evident from the topography images acquired by AFM, shown in Fig. 5a–d. Again, the surface of CS/PEGDE coatings is relatively smooth, with no important changes in roughness. Instead, in nanocomposite coatings, high roughness variations characterized by the typical polygonal shape of GO nanoplate aggregates were observed, with larger clusters dimension of about 1 μm and 2 μm for 1 wt% and 2 wt% of GO in the CS matrix, respectively (Fig. 5c–d). Fig. 5e shows the cross-sectional TEM image of GO-containing samples, where the nanoplates appear oriented along the coating surface. This result demonstrated that the ultrasonic spray coating technique effectively promotes an oriented layered morphology of 2D nanofillers dispersed in the chitosan matrix, thanks also to the production of very thin coating layers (about 800 nm).

3.4. Mechanical characterization of coatings

The mechanical properties of the coatings were evaluated by conducting nanoindentation and nanoscratch tests to determine the impact of both GO addition and formation of coating by layer deposition. Fig. 6a–b report representative loading-unloading nanoindentation curves and maximum penetration depth statistical distribution. The

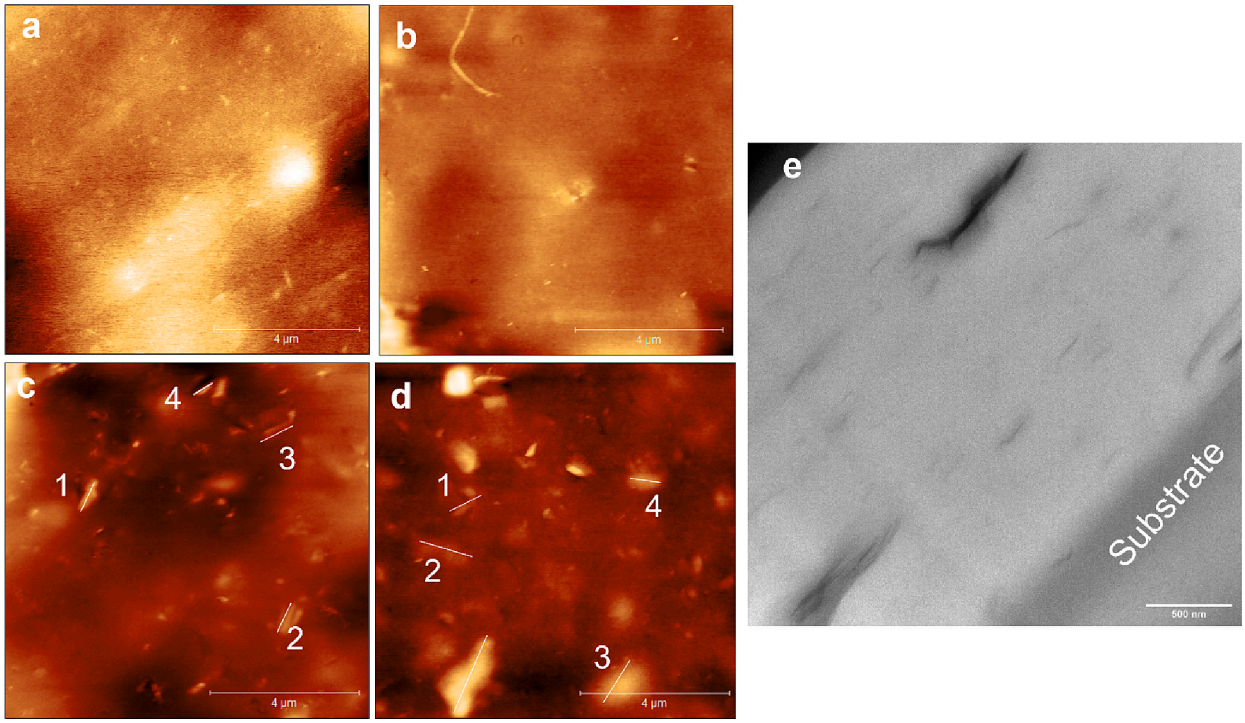

Fig. 5. AFM height images of 3 L CS/PEGDE (a), and CS/PEGDE/GO coatings films prepared by varying GO content: 0.5 wt% (b), 1 wt% (c), 2 wt% (d). Representative Transmission Electron Microscope image of 3-layer coatings with 1 wt% GO, where the substrate is represented by the PBS film (e).

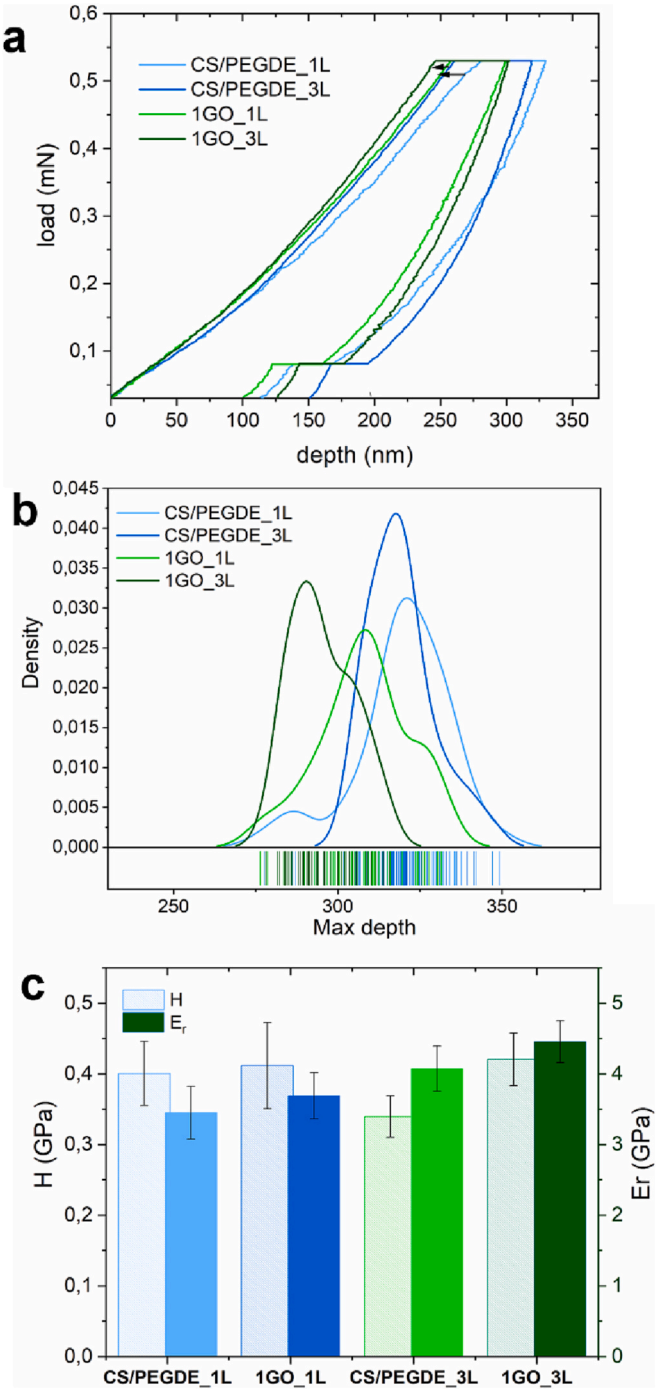

Fig. 6. Representative loading-unloading curves (a), maximum depth distribution (b), reduced modulus and hardness (c) from nanoindentation tests of 1-layer and 3-layer CS/PEGDE and CS/PEGDE/GO coatings.

presence of GO increases the resistance to the applied load of the CS/PEGDE coatings since higher loads are needed to reach the same penetration depth. Furthermore, comparing the nanocomposite coatings with different thicknesses, it is worth noticing that the tri-layer structure displayed a higher resistance and a narrower distribution of the maximum penetration depth. As observed in a previous work of some of the authors [46], this result indicated that the deposition of overlapping layers provides a more compact and homogeneous distribution of GO nanoplates along the coating surface. Furthermore, the hardness and reduced elastic modulus values of monolayer coatings (CS/PEGDE and CS/PEGDE/GO) are similar, while the properties are significantly improved for the tri-layer coatings. Also, the reduced modulus increases with the number of layers in the coatings containing GO.

The coatings scratch resistance showed a similar response to the presence of GO. The results of the measurements are displayed in Fig. 7a–b, which depicts representative optical micrographs of the scratch paths, as well as the corresponding penetration depth vs displacement profile curves. The monolayer CS/PEGDE coatings display high penetration depth at low applied loads, and are characterized by a significant pile-up deformation mechanism, as demonstrated by the curve trend [46]. Despite the tri-layer CS/PEGDE coatings showing a lower plastic deformation during the nanoscratch experiments, the critical load (that corresponds to the load value at which the primary fracture phenomenon is observed [47]) is very similar to the monolayer samples (approximately equal to 5 mN). A significant improvement in scratch resistance for coatings containing GO is observed, as evidenced by the higher critical load compared to the samples without GO. Moreover, the tri-layer structure turns out to be more performing, with an increase of the critical load from around 8 mN for the monolayer to 15 mN for the tri-layer samples.

The coating adhesion was assessed through the cross-cut test, in accordance with the ISO 2409 standard. Fig. 7c shows the coating's appearance after removing the tape. The tri-layer coatings containing GO showed only modest flaking along cut edges, which identifies a suitable adhesion (i.e. adhesion quality of 2 on a 0–5 scale determined by the standard). However, the monolayer coatings do not show any loss of material, suggesting that the overlapping of several layers slightly reduces the coating adhesion. Instead, the CS/PEGDE coatings display a loss of coating material along the cuts' blades and squares, which may be ascribed to the intrinsic lower mechanical resistance of the pristine coatings, without the reinforcing effect of GO.

The nanocomposite coatings do not significantly affect the mechanical properties of the PBS substrate. However, it is worth considering that the strain at break of the specimens with chitosan coatings is slightly reduced with respect to the pristine PBS, while the presence of GO coatings helps to keep the initial value of PBS unchanged (Table S3). This evidence is important since PBS is selected as a substrate for making effective flexible packaging precisely on the basis of deformation at break.

3.5. Gas transmission rate of coated PBS films

To evaluate the gas barrier properties of the CS/PEGDE and CS/PEGDE/GO-coated PBS films, the oxygen and carbon dioxide transmission rates (OTR and CO_2TR) were measured. The results of the measurements are presented in Fig. 8. The test was performed at 5 % and 50 % relative humidity (RH) at 25 °C: by increasing the number of deposited layers and the coating thickness, the OTR and CO2TR decreasing. Furthermore, the addition of GO up to 1 % *w*/w resulted in an improvement in the barrier properties. The decrease in gas transmission observed with the addition of GO to the CS matrix, as well as with an increase in GO content, can be attributed to the reduced solubility of gas molecules (since GO nanoplates are impermeable to gas molecules) and the formation of a highly oriented nanoplate morphology. This morphology creates a more tortuous pathway for the penetration of gas molecules [48]. It should be noted that further increasing the GO concentration to 2 % w/w actually results in an increase in OTR and CO_2TR, which indicates a deterioration of the gas barrier performance. This is ascribed to increased aggregate particles observed from the morphological characterization. The heterogeneous distribution of GO provides a less compact structure with the same number of layers deposited (Table S2), reducing the tortuous paths and facilitating gas molecule penetration. The reduction of both OTR and CO_2TR is less significant at 50 % relative humidity. The best-performing 2,5 μm thick tri-layer structure in dry conditions can reduce the OTR and CO_2TR by 85 % and 93 %, respectively, compared with pristine PBS film. Instead, at 50 % RH, the same coating imparts an OTR and CO_2TR

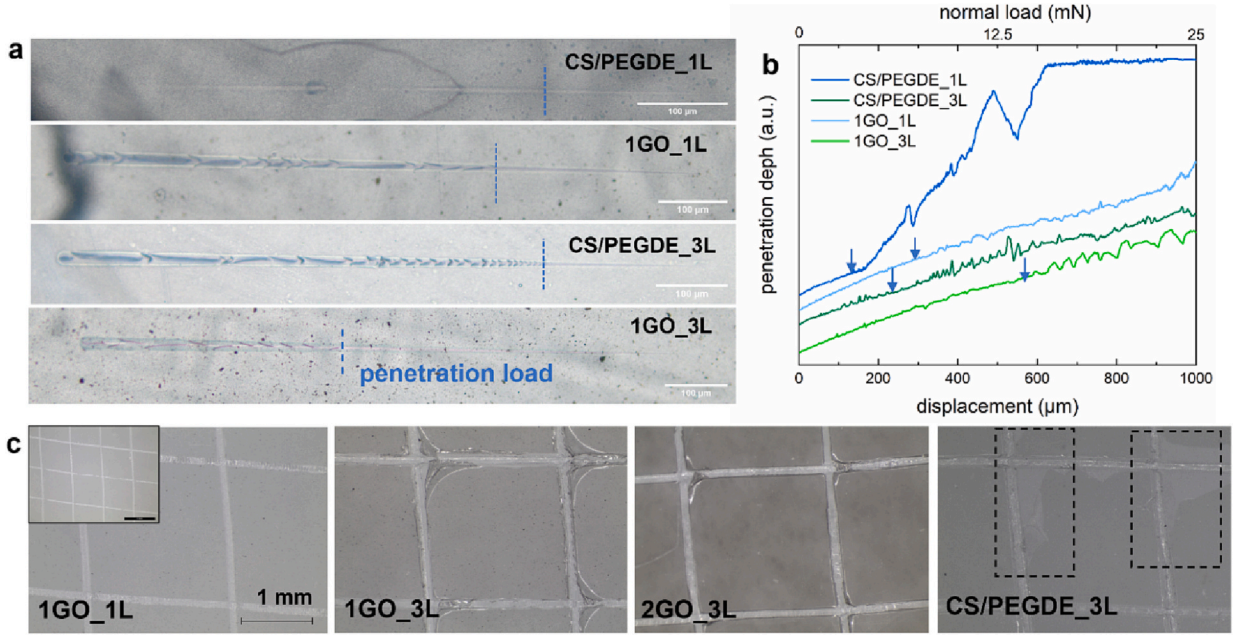

Fig. 7. Representative optical micrographs of the scratches (a) and corresponding penetration deph vs displacement curves (b). The arrows refer to the critical load and correspond to the vertical blue lines drawn in the optical micrographs. The scratch direction is from right to left. Representative optical micrographs show the coating surface's appearance after the cross-cut adhesion tests (c). (For interpretation of the references to colour in this figure legend, the reader is referred to the web version of this article.)

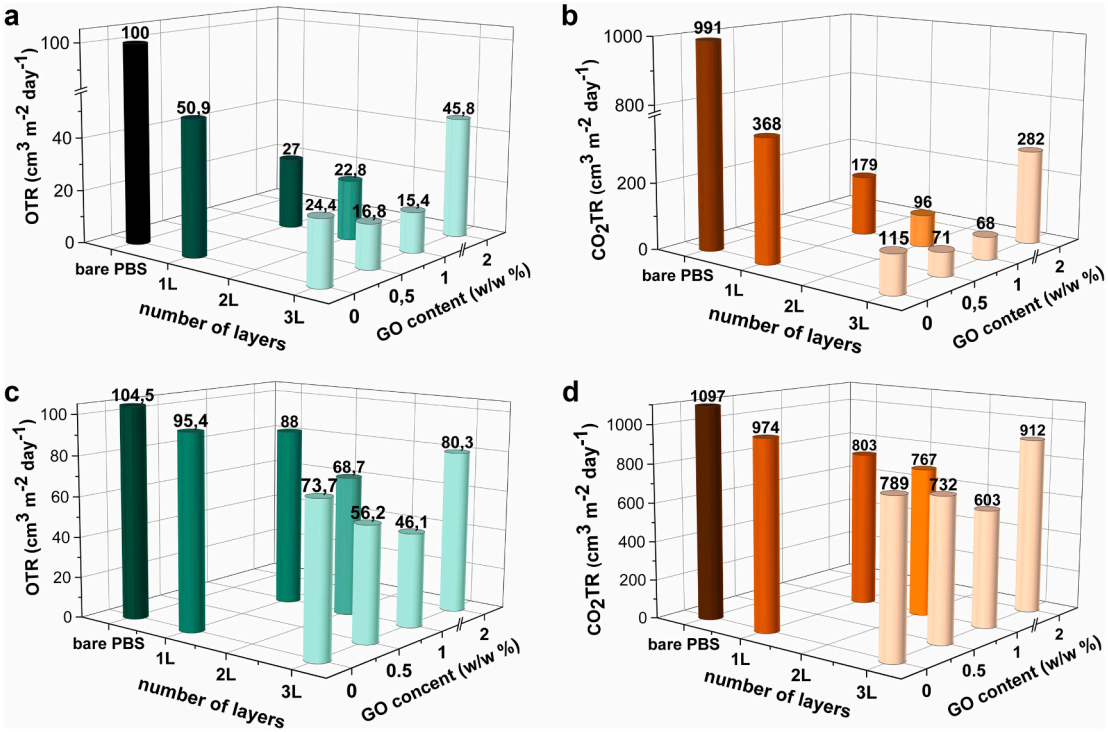

Fig. 8. Gas Barrier properties of coated films against the number of layers and GO content. CO_2TR measured at 5 % (a) and 50 % (c) of RH. OTR measured at 5 % (b) and 50 % (d) of RH.

reduction by about 45 % and 56 %, respectively. This loss in terms of barrier performance is ascribed to the hydrophilic nature of CS and GO. In fact, despite the crosslinked network drastically reducing the water uptake of the CS/GO composite, it still allows for incorporating a certain amount of water between the polymer chains. The adsorbed water molecules act as a plasticizer and affect the available diffusion volume for gas, leading to increased OTR and CO_2TR values [49].

To further assess the potential of USS coating technology for producing homogeneous gas barrier nanocomposite coatings, a comparison was made with the air-spray coating process. In Fig. S7c, the typical surface appearance of coatings deposited by air-spray coater is shown. The distribution of the coating material appears much less homogeneous

than that of the coatings obtained via USS coating (Fig. S7a), with some aggregate particles of the coating mixture distributed over the surface of the coated film. In turn, the oxygen permeability measured at 5 % RH of the coating prepared by air-spray, equal to 9.08 [cc·mm·m^{-2}·day^{-1} atm], turns out to be 3 times greater than that of the monolayer coating deposited by ultrasonic spray (Table S3). These results highlight the effectiveness of the ultrasonic spray technology to ensure a homogeneous distribution of the developed mixture and to improve the gas barrier properties of the deposited coating.

In order to gain a better understanding of the potential of the obtained coatings, the ratio between CO_2TR and OTR is illustrated in Fig. 9. The pristine PBS films exhibit a CO_2TR/OTR ratio of about 10, whereas, for the coated films, the value progressively decreases with the number of deposited layers, achieving a ratio of around 5 for the 3-layer coated films. This finding demonstrated that the CS/PEGDE/GO coatings exhibit a greater barrier effect on carbon dioxide than on oxygen. Santosh Kumar et al. [50] and Nazrul Hsan et al. [51] also have previously shown the high CO_2 absorption capacity of the CS/GO system. This effect was attributed to the high number of amine groups that interact with CO_2 molecules, as well as the large surface area of GO plates. The observed variation in permselectivity allows for the tuning of the gas barrier properties ratio of the coatings. It also suggests the application of the developed coatings in fields where different permselectivity intervals are required, such as packaging in a modified atmosphere (MAP) [52]. In this case, a high concentration of carbon dioxide in the internal atmosphere of food packaging (e.g. package of bakery products [53] is generally exploited to extend the food shelf-life.

Oxygen permeability (OP) and oxygen permeability reduction (Table S4 and S5) of the obtained coatings were benchmarked to barrier properties of coatings selected from literature and market. Although gas barrier layers used within the food packaging industry (i.e., EVOH, metalized plastics) still provide a lower oxygen permeability, they are not bio-based and are difficult to be recycled. Therefore, developing environmentally friendly and water-based coatings from natural sources is highly desirable to promote the application of coated biodegradable packaging in a circular economy context [1].

4. Conclusions

The present study successfully deposited chitosan-based nanocomposite gas barrier coatings onto a compostable PBS film using the USS coating deposition technique with a negligible loss the film transparency. The water swelling resistance of the hydrophilic chitosan matrix was improved by the crosslinking reaction between PEGDE and the amino groups of CS, which led to a water uptake reduction of 96 %. The CS/PEGDE/GO nanocomposite coating with 1 wt% of GO and 2.4 μm thick allowed to achieve OTR and CO_2TR reductions of 85 % and 93 %, respectively, as compared with uncoated PBS films. Furthermore, the improvement in CO_2 barrier properties was significantly higher than that related to oxygen (two times more for the tri-layer coatings), suggesting the use of the developed coatings where different permeation rates of the two gases are required. The improvement in gas permeability was correlated to the formation of highly oriented morphology of GO nanoplates and compact, densely packed coating layers. The mechanical characterization revealed an effective adhesion of the coatings to the PBS films and improved mechanical and scratch resistance thanks to the addition of GO nanofillers.

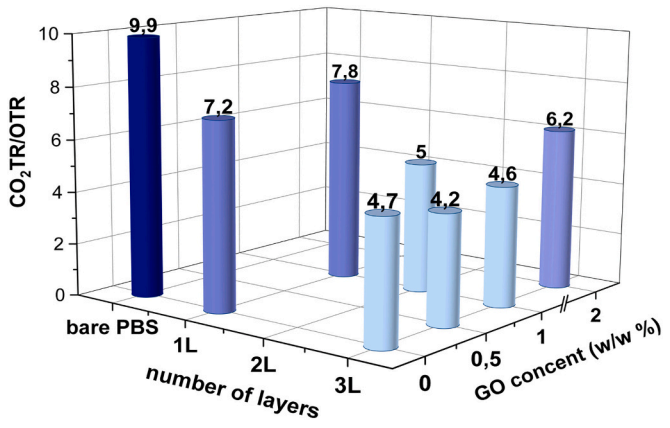

Fig. 9. CO_2TR/OTR ratio of coated films as a function of the number of deposited layers and GO content measured at 5 % RH and 25 °C.

This research provides a significant perspective on the USS coating technique's potential for producing barrier bio-nanocomposite coatings on flexible plastic films, guaranteeing elevated process speed and scalability, accurate control of coating morphology and nanofiller orientation, and coating thickness in the micrometer range. Furthermore, the use of a renewable and biodegradable natural polymer as a coating matrix and the incorporation of a minimal amount of nanofiller (ϵ 1.2* 10^{-6} g/cm^2) helps maintain the sustainable character of the coated film, while achieving improved oxygen and carbon dioxide barrier performance. Thus, the proposed approach may be an effective strategy to improve the application range of compostable films and move towards mono-material packaging solution, that represents a more sustainable end-of-life option for plastic-based flexible packaging.

Fundings

This work has been supported by the project "sPATIALS3" (ID 1176485) Regione Lombardia under the ROP ERDF2014–2020—Axis I–Call Hub Ricerca e Innovazione.

Funding from the EU H2020 CE-BG-06-2019 project "Developing and Implementing Sustainability-Based Solutions for Bio-Based Plastic Production and Use to Preserve Land and Sea Environmental Quality in Europe - BIO-PLASTICS EUROPE", grant agreement ID: 860407 is also acknowledged.

LDN carried out this study within the Agritech National Research Center and received funding from the European Union Next-GenerationEU (PIANO NAZIONALE DI RIPRESA E RESILIENZA (PNRR) – MISSIONE 4 COMPONENTE 2, INVESTIMENTO 1.4 – D.D. 1032 17/06/2022, CN00000022). The authors would also like to acknowledge the Coordenação de Aperfeiçoamento de Pessoal de Nível Superior (CAPES) for the grant PRINT 88887.310339/2018–00, and the Mackenzie Research Fund (MackPesquisa, Project number 181009).

This manuscript reflects only the authors' views and opinions, neither the European Union nor the European Commission can be considered responsible for them.

CRediT authorship contribution statement

Alessia Cabrini: Investigation, Methodology, Formal analysis, Data curation, Writing – original draft. **Arash Ghalayani Esfahan:** Data curation, Writing – review & editing. **André Petraconi:** Investigation. **Marino Lavorgna:** Supervision, Funding acquisition, Conceptualization, Writing – review & editing. **Luigi De Nardo:** Resources, Funding acquisition, Writing – review & editing. **Giovanna Buonocore:** Resources, Funding acquisition. **Ricardo Jorge Espanhol Andrade:** Resources, Supervision. **Pierfrancesco Cerruti:** Resources, Supervision, Funding acquisition, Writing – review & editing.

Declaration of competing interest

The authors declare that they have no known competing financial interests or personal relationships that could have appeared to influence the work reported in this paper.

Data availability

No data was used for the research described in the article.

Acknowledgments

The authors would like to acknowledge Corapack S.r.l. (Brenna (CO), Italy) for providing BioPBS substrates. The authors also thank Mr. Mario De Angioletti, Mrs. Cristina Del Barone for providing technical support.

Appendix A. Supplementary data

Supplementary data to this article can be found online at https://doi.org/10.1016/j.porgcoat.2023.107760.

References

[1] F. Wu, M. Misra, A.K. Mohanty, Challenges and new opportunities on barrier performance of biodegradable polymers for sustainable packaging, Prog. Polym. Sci. 117 (2021), 101395, https://doi.org/10.1016/j.progpolymsci.2021.101395.
[2] S. Mangaraj, A. Yadav, L.M. Bal, S.K. Dash, N.K. Mahanti, Application of biodegradable polymers in food packaging industry: a comprehensive review, Journal of Packaging Technology and Research 3 (2019) 77–96.
[3] A.R. de Matos Costa, A. Crocitti, L.H. de Carvalho, S.C. Carroccio, P. Cerruti, G. Santagata, Properties of biodegradable films based on poly (butylene succinate) (PBS) and poly (butylene Adipate-co-terephthalate) (PBAT) blends, Polymers 12 (2020) 2317.
[4] J. Xu, B.H. Guo, Poly (butylene succinate) and its copolymers: research, development, and industrialization, Biotechnol. J. 5 (2010) 1149–1163.
[5] G. Guidotti, M. Soccio, V. Siracusa, M. Gazzano, E. Salatelli, A. Munari, N. Lotti, Novel random PBS-based copolymers containing aliphatic side chains for sustainable flexible food packaging, Polymers 9 (2017) 724.
[6] C. Vasile, Polymeric nanocomposites and Nanocoatings for food packaging: a review, Materials 11 (1834) 2018, https://doi.org/10.3390/ma11101834.
[7] P. Tyagi, K.S. Salem, M.A. Hubbe, L. Pal, Advances in barrier coatings and film technologies for achieving sustainable packaging of food products – a review, Trends Food Sci. Technol. 115 (2021) 461–485.
[8] M.Z. Khajavi, A. Ebrahimi, M. Yousefi, S. Ahmadi, M. Farhoodi, A.M. Alizadeh, M. Taslikh, Strategies for producing improved oxygen barrier materials appropriate for the food packaging sector, Food Eng. Rev. 12 (2020) 346–363.
[9] J. You, B. Oh, Y.S. Yun, H. Jin, Improvement in barrier properties using a large lateral size of exfoliated graphene oxide, Macromol. Res. 28 (8) (2020) 709–713.
[10] S.P. Damari, L. Cullari, R. Nadiv, Y. Nir, D. Laredo, J. Grunlan, O. Regev, Graphene-induced enhancement of water vapor barrier in polymer nanocomposites, Composites Part B 134 (2018) 218–224.
[11] I.U. Unalan, D. Boyacı, M. Ghaani, S. Trabattoni, S. Farris, Graphene oxide bionanocomposite coatings with high oxygen barrier properties, Polymers 8 (2016) 246–255.
[12] H. Chiang, T.J. Kolibaba, B. Eberle, J.C. Grunlan, Super gas barrier of a polyelectrolyte/clay Coacervate thin film, Macromol. Rapid Commun. 2000540 (2020).
[13] M. Salzano de Luna, Y. Wang, T. Zhai, L. Verdolotti, G.G. Buonocore, M. Lavorgna, H. Xia, Nanocomposite polymeric materials with 3D graphene-based architectures: from design strategies to tailored properties and potential applications, Prog. Polym. Sci. 89 (2019) 213–249.
[14] M. Mujtaba, R.E. Morsi, M.Z. Garry Kerch, M. Elsabee, J. Kaya, K. Labidi, M. Khawar, Current advancements in chitosan-based film production for food technology; a review, Int. J. Biol. Macromol. 121 (2019) 889–904.
[15] P. Cazón, M. Vázquez, Mechanical and barrier properties of chitosan combined with other components as food packaging film, Environ. Chem. Lett. 18 (2020) 257–267, https://doi.org/10.1007/s10311-019-00936-3.
[16] K. Kosowskaa, P. Domalik-Pyzika, M. Nocuńb, J. Chłopeka, Chitosan and graphene oxide/reduced graphene oxide hybrid nanocomposites – evaluation of physicochemical properties, Mater. Chem. Phys. 216 (2018) 28–36.
[17] B. Qu, Y. Luo, A review on the preparation and characterization of chitosan-clay nanocomposite films and coatings for food packaging applications, Carbohydrate Polymer Technologies and Applications 2 (2021), 100102.
[18] G. Laufer, C. Kirkland, Amanda A. Cain, J.C. Grunlan, Clay–Chitosan Nanobrick Walls: Completely Renewable Gas Barrier and Flame-Retardant Nanocoatings, ACS Appl. Mater. Interfaces 4 (3) (2012) 1643–1649.
[19] P. Majumdera, R. Gangopadhyay, Evolution of graphene oxide (GO)-based nanohybrid materials with diverse compositions: an overview, RSC Adv. 12 (9) (2022) 5686–5719.
[20] N. Yan, F. Capezzuto, M. Lavorgna, G.G. Buonocore, F. Tescione, H. Xia, L. Ambrosio, Borate cross-linked graphene oxide–chitosan as robust and high gas barrier films, Nanoscale 8 (20) (2016) 10783–10791.
[21] J. Ahmed, M. Mulla, Y.A. Arfat, T.L.A. Thai, Mechanical, thermal, structural and barrier properties of crab shell chitosan/graphene oxide composite films, Food Hydrocoll. 71 (2017) 141–148, https://doi.org/10.1016/j.foodhyd.2017.05.013.
[22] F. Han Lyn, C.P. Tan, R.M. Zawawi, Z.A. Nur Hanani, Enhancing the mechanical and barrier properties of chitosan/graphene oxide composite films are enhanced using trisodium citrate and sodium tripolyphosphate crosslinkers, J. Appl. Polym. Sci. 138 (2021), e50618, https://doi.org/10.1002/app.50618.
[23] M.G. Chuc-Gamboa, R.F. Vargas-Coronado, J.M. Cervantes-Uc, J.V. Cauich-Rodríguez, D.M. Escobar-García, A. Pozos-Guillén, J. San Román del Barrio, The effect of PEGDE concentration and temperature on physicochemical and biological properties of chitosan, Polymers 11 (2019) 1830, https://doi.org/10.3390/polym11111830.
[24] H. Tanuma, T. Saito, K. Nishikawa, T. Dong, K. Yazawa, Y. Inoue, Preparation and characterization of PEG-cross-linked chitosan hydrogel films with controllable swelling and enzymatic degradation behaviour, Carbohydr. Polym. 80 (2010) 260–265.
[25] O. Catanzano, G. Gomez d'Ayala, A. D'Agostino, F. Di Lorenzo, C. Schiraldi, M. Malinconico, R. Lanzetta, F. Bonina, P. Laurienzo, PEG-crosslinked-chitosan hydrogel films for in situ delivery of Opuntia ficus-indica extract, Carbohydr. Polym. 264 (2021), 117987.
[26] CFR - Code of Federal Regulations Title 21. Code Fed. Regul. https://www.accessdata.fda.gov/scripts/cdrh/cfdocs/cfcfr/CFRSearch.cfm?fr=178.3750 (accessed: August 30, 2022).
[27] S. Qin, Y. Song, M.E. Floto, J.C. Grunlan, Combined high Stretchability and gas barrier in hydrogen-bonded multilayer Nanobrick Wall thin films, ACS Appl. Mater. Interfaces 9 (2017) 7903–7907.
[28] F. Li, M. Paolo Biagioni, S. Finazzi, L. Piergiovanni Tavazzi, Tunable green oxygen barrier through layer-by-layer self-assembly of chitosan and cellulose nanocrystals, Carbohydr. Polym. 92 (2013) 2128–2134.
[29] J. Heo, M. Choi, J. Hong, Facile surface modification of polyethylene film via spray-assisted layer-by-layer self-assembly of graphene oxide for oxygen barrier properties, Sci. Rep. 9 (2019) 2754.
[30] M. Dobre, L. Bolle, Practical design of ultrasonic spray devices: experimental testing of several atomizer geometries, Exp. Thermal Fluid Sci. 26 (2002) 205–211.
[31] K. Sreeja Sadanandan, A. Bacon, D.W. Shin, S.F.R. Alkhalifa, S. Russo, M. F. Craciun, A.I.S. Neves, Graphene coated fabrics by ultrasonic spray coating for wearable electronics and smart textiles, J. Phys. Mater. 4 (2021), 014004.
[32] S. Bose, S. Stephan, S. Keller, T.S. Alstrøm, A. Boisen, K. Almdal, Process optimization of ultrasonic spray coating of polymer films, angmuir 29 (2013) 6911–6919.
[33] M. Bastwros, G.Y. Kim, Ultrasonic spray deposition of SiC nanoparticles for laminate metal composite fabrication, Powder Technol. 288 (2016) 279–285.
[34] S. Slegers, M. Linzas, J. Drijkoningen, J. D'Haen, N.K. Reddy, W. Defame, Surface roughness reduction of additive manufactured products by applying a functional coating using ultrasonic spray coating, Coatings 7 (12) (2017) 208, https://doi.org/10.3390/coatings7120208.
[35] T. Thornber, O.S. Game, E.J. Cassella, M.E. O'Kane, J.E. Bishop, T.J. Routledge, T. I. Alanazi, M. Today, P.J.M. Isherwood, L.C. Infante-Ortega, D.B. Hammond, J. M. Walls, D.G. Lidzey, Nonplanar spray-coated perovskite solar cells, ACS Appl. Mater. Interfaces 14 (3) (2022) 37587–37594.
[36] B. Modesto-López, M. Miettinen, T. Torvela, A.L.J. Jokiniemi, Direct deposition of graphene nanomaterial films on polymer-coated glass by ultrasonic spraying, Thin Solid Films 578 (2015) 45–52.
[37] M. Abbas, M. Buntinx, W. Defame, N. Reddy, R. Peeters, Oxygen gas and UV barrier properties of Nano-ZnO-coated PET and PHBHHx materials fabricated by ultrasonic spray-coating technique, Nanomaterials 11 (2021) 449, https://doi.org/10.3390/nano11020449.
[38] H. Kiuchi, W. Kai, Y. Inoue, Preparation and characterization of poly(ethylene glycol) crosslinked chitosan films, J. Appl. Polym. Sci. 107 (2008) 3823–3830.
[39] M. Lavorgna, F. Piscitelli, P. Mangiacapra, G.G. Buonocore, Study of the combined effect of both clay and glycerol plasticizer on the properties of chitosan films, Carbohydr. Polym. 82 (2010) 291–298.
[40] N. Li, R. Bai, A novel amine-shielded surface cross-linking of chitosan hydrogel beads for enhanced metal adsorption performance, Ind. Eng. Chem. Res. 44 (17) (2005) 6692–6700.
[41] P. Guerrero, A. Muxika, I. Zarandona, K. de la Caba, Crosslinking of chitosan films processed by compression molding, Carbohydr. Polym. 206 (2019) 820–826.
[42] E. Vassallo, M. Aloisio, M. Pedroni, F. Ghezzi, P. Cerruti, R. Donnini, Effect of low-pressure plasma treatment on the surface wettability of poly(butylene succinate) films, Coatings 12 (2022) 220.
[43] V.G. Lauriano Souza, I. Penido Mello, O. Khalid, J.R. Afonso Pires, C. Rodrigues, M. M. Alves, C. Santos, A.L. Fernando, I. Coelhoso, Strategies to improve the barrier and mechanical properties of pectin films for food packaging: comparing nanocomposites with bilayers, Coatings 12 (2) (2022) 108.
[44] Y. Zhan, Y. Meng, Y. Li, C. Zhang, Q. Xie, S. Wei, M. Lavorgna, Z. Chen, Poly (vinyl alcohol)/reduced graphene oxide multilayered coatings: the effect of filler content on gas barrier and surface resistivity properties, composites, Communications 24 (2021) 100670.
[45] Y. Pan, T. Wu, H. Bao, L. Li, Green fabrication of chitosan films reinforced with parallel aligned graphene oxide, Carbohydr. Polym. 83 (4) (2011) 1908–1915.
[46] M. Mihelčič, M. Gaberšček, M. Salzano de Luna, M. Lavorgna, C. Giuliani, G. Di Carlo, A.K. Surca, Effect of silsesquioxane addition on the protective performance of fluoropolymer coatings for bronze surfaces, Mater. Des. 178 (2019), 107860.
[47] C. Yu, M. Sulzano de Luna, A. Marotta, C. Ponti, I. Esposito, F. Scherillo, Z. Wang, X. Zhang, H. Xia, M. Lavorgna, NIR light-triggered self-healing waterborne polyurethane coatings with polydopamine-coated reduced graphene oxide nanoparticles, Progress in Organic Coatings 161 (2021), 106499.
[48] J. Yu, K. Ruengkajorn, D. Georgiana Crivoi, C. Chen, J.C. Buffet, D. O'Hare, High gas barrier coating using non-toxic nanosheet dispersions for flexible food packaging film, Nat. Commun. 10 (2019) 2398.

[49] S. Lazar, O. Garcia-Valdez, E. Kennedy, P. Champagne, M. Cunningham, J. Grunlan, Crosslinkable-chitosan-enabled moisture-resistant multilayer gas barrier thin film, Macromol. Rapid Commun. 40 (2019) 1800853.
[50] N. Hsan, P.K. Dutta, S. Kumar, R. Bera, N. Das, Chitosan grafted graphene oxide aerogel: synthesis, characterization and carbon dioxide capture study, Int. J. Biol. Macromol. 125 (2019) 300–306.
[51] S. Kumar, M.Y. Wani, J. Koh, J.M. Gil, Abilio J.F.N. Sobral, Carbon dioxide adsorption and cycloaddition reaction of epoxides using chitosan–graphene oxide nanocomposite as a catalyst, J. Environ. Sci. 69 (2018) 77–84, https://doi.org/10.1016/j.jes.2017.04.013.
[52] K. Czerwinski, T. Rydzkowski, J. Wróblewska-Krepsztul, V. Kumar Thakur, Towards impact of modified atmosphere packaging (MAP) on shelf-life of polymer-film-packed food products: challenges and sustainable developments, Coatings 11 (2021) 1504, https://doi.org/10.3390/coatings11121504.
[53] O.J. Caleb, P.V. Mahajan, F. Al-Julanda Al-Said, U. Linus Opa, Modified atmosphere packaging Technology of Fresh and Fresh-cut Produce and the microbial consequences—a review, Food Bioprocess Technol. 6 (2013) 303–329.